lajss.org
Latin American Journal of Solids and Structures
www.lajss.org

A Faster Method for Evaluating the Ultimate Strength of Ship Hulls Under Elevated Temperatures - Fire Idealized Structural Unit Method

Jiaxin Wu [a] 0009-0005-2797-7932, Ming Yan [a*] 0000-0002-8793-3510, Xingwei Sun [a] 0000-0002-8473-8613

[a] Liaoning Shock Protection and Damage Assessment Technology Engineering Research Center, Shenyang University of Technology, Shenyang 110780, China. Email wujiaxin@smail.sut.edu.cn, yanming7802@163.com, sunxingw@126.com

* Corresponding author

Abstract

An easier and more efficient method is proposed for evaluating the ultimate strength of ship structures under fire conditions. Based on the Ideal Structural Unit Method (ISUM) and experiments from reference literature, a stress and strain equation for stiffened plates under fire conditions, as well as Fire ISUM, are proposed. To verify the effectiveness of the Fire ISUM method, 48 sets of FEA simulations incorporating the Fire ISUM were used to calculate the ultimate strength of different cabin fire positions and temperatures. The results showed that both the simulation and Fire ISUM were able to evaluate the high temperature ultimate strength. However, the Fire ISUM method does not account for initial imperfections due to the use of ideal high-temperature stress-strain curves. As a result, simulation results are lower than those obtained with the Fire ISUM, with a maximum error of 5.24%. To study the influence mechanism of ultimate strength of ship under high temperature conditions, the ultimate strength attenuation factor "I_{UR}" was defined. Simulation results show that the ultimate strength attenuation of different cabins is not only related to the high-temperature width but also to the distance between the deck and the neutral axis. In actual fire rescue processes, when a deck of the same area is subjected to high temperatures, the further the deck is from the neutral axis, the more important its protection.

Keywords

Ultimate Strength; Residual Strength; Ship fire; ISUM; Fire ISUM;

Graphical Abstract

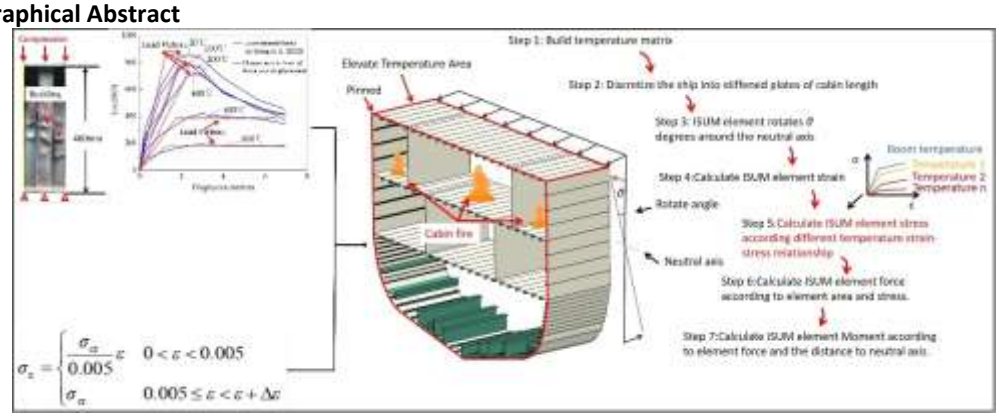

1 INTRODUCTION

Ships play a crucial role in trade and transportation, so protecting and improving the safety of the hull to ensure its safe operation is of great significance. Currently, ships are facing various threats, according to the International Maritime Organization (IMO) (2004), fire&explosion is one of the initial incidents and assigned to reviewers to casualty analysis, this indirectly indicates that the hazards of fire and explosion need to be taken seriously. Several ship fire accidents that have occurred in the past, further demonstrate the hazards of fire and explosion. On 12 July, 2020, according to CNN reporter LAGRONE (2020), 21 individuals were injured after an explosion and fire on the USS Bonhomme Richard at the dock of the San Diego Naval Base in Figure 1. There are similar cases as well, Lendon (2024) reported that the Minsk burned in a waterway. According to the MSC Capetown III report by the Sri Lanka Ports Authority (2024), a fire broke out and subsequently led to an explosion. The South African Maritime Safety Authority (SAMSA) (2024) reported that an offshore supply vessel, the AM Pride, caught fire. In previous studies, many researchers have also provided statistics on ship fire accidents that have already occurred (Baalisampang et al., 2018; Wang et al., 2020; Callesen et al., 2021; Krmek et al., 2022). These studies also demonstrate the hazards of ship fires. Wu et al. (2024) analyzed casualty provided by EMSA from 2020 to 2022 in pointed out that, although EMSA did not specifically mention the number of accidents, the data suggests that explosion and fire incidents may potentially increase in recent years. Figure 2 shows the number of accident casualties from 2020 to 2022 provided by EMSA. The causes of accidents include collision, flooding/sounding, capsizing/listing, fire/explosion, and damage/loss of equipment. When comparing the data for fire/explosion accidents with the other four types, it becomes evident that the number of accidents involving explosions and fires gradually increased from 2020 to 2022. Notably, in 2022, the number of casualties from explosions and fires was twice as many as those from the other four types of accidents combined. According to EMSA data and reports of recent ship fire accidents, the number has been increasing, causing serious personnel and property losses. Therefore, this topic holds significant research value for ship fires.

Figure 1: USS Bonhomme Richard ship fire at the dock of the San Diego Naval Base

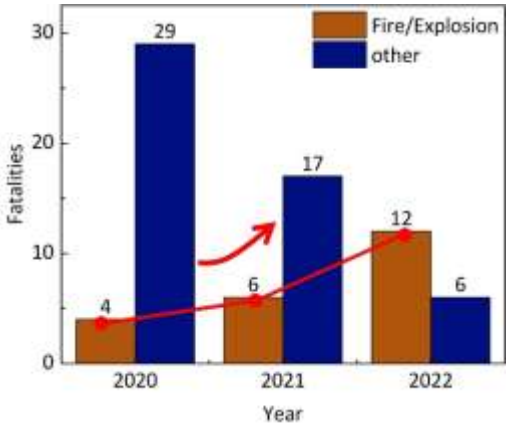

Figure 2: EMSA data indicate explosions and fires caused higher casualties than other types of accidents in 2022.

Frequent ship fires also pose a great threat to the ultimate strength of the ship, causing concern among scholars. Therefore, scholars have conducted research to evaluate the ultimate strength of the ship under fire conditions. From the perspective of the method for evaluating the ultimate strength of ships under fire conditions, full-scale fire tests can accurately and intuitively reflect the failure modes and mechanical characteristics under fire conditions. J.K. Paik et al. (2021) conducted full-scale stiffened plate fire tests to study the deformation and failure modes of vertical stiffened plate compression under fire conditions, providing a reference for the study of ship ultimate strength under fire conditions. However, the large scale involved in full-scale ship fire tests poses challenges in terms of fire loading and data measurement. Consequently, there are few ship fire tests conducted currently. The finite element method is a common method for calculating the ultimate strength of ship hulls. Ryu M.G. et al. (2021) used simulation calculations to verify the experiments and analyses conducted by J.K. Paik, focusing on how different temperature fires impact the ultimate strength of stiffened plates, and verified the feasibility of studying ship damage under fire conditions. To improve the fire resistance design of ships, Guo et al. (2023) used simulation to evaluate the residual strength of ship hull with fire conditions and varying heat release rates (HRR). Li et al. (2019) using thermal radiation method as fire boundary conditions to conduct engine room fires simulation and studied the impact on the ultimate strength of the ship. Liu et al. (2022) studied non-uniform multi-cabin fires, proposed a forecasting model for the vessel ultimate strength under fire

conditions, and found higher the heat release rates, the smaller the residual strength. Table 1 shows the details of researchers evaluating the ultimate strength of ship hulls under fire conditions.

Table 1 Researchers evaluate the details of the ultimate strength of ship fires

Author	Method Description	Geometric Nonlinear& Material Nonlinear	Initial Geometric Imperfections	fire dynamics conditions or simply elevated temperature	CFD Simulati-on
Paik et al. (2021)	Based on the ISO-834 fire test, conduct experimental analysis on the ultimate fire strength of stiffened panels.	Yes	No	Fire Dynamics	No
Ryu M.G. et al. (2021)	Based on Paik et.al experiment conduct FEM analysis.	Yes	No	Simply Elevated Temperature	No
Guo et al. (2023)	Based on the use of large eddy simulation for fire dynamics and structural thermal coupling methods.	Yes	No	Fire Dynamics	Yes
Li et al. (2019)	Based on dual zone large eddy and structural thermal coupling methods.	Yes	No	Fire Dynamics	Yes
Liu et al. (2022)	Based on large eddy simulation of fire dynamics algorithm and the structural thermo-mechanical coupling response method.	Yes	No	Fire Dynamics	Yes

However, the nonlinear analysis of large structures using the finite element method requires large amounts of modeling work and computational time. To solve this problem, scholars strive to reduce the modeling work and computation time of structural non-linear analysis. The most effective way to reduce this workload and computational time is to reduce the degrees of freedom. For the fields of structural engineering, scholars have proposed some theoretical methods for rapid assessment of structure's ultimate strength. Machado et al. (2020) proposed a new prediction model for assessing the stability of reinforced concrete panels in fire with limit analysis theory. R. Schardt (1989) applicability of the Generalized Beam Theory (GBT) which aimed at reducing computational effort by minimizing degrees of freedom. Bebiano, R (2018) highlights the development of a graphical interface for GBT-based analyses, providing insights into buckling and vibration behaviors of thin-walled members. Barichello et al. (2017) used the GBT method to select the geometric shape of the beam and conducted buckling/branching analysis using GBTul code. At same time apply DSM encoding method for comparison with numerical data of ultimate bending moment. Barichello et al. pointed out that in the range of medium to high slenderness ratios, the predictions provided by the DSM torsion strength curve are mostly unsafe. Y. K. Cheung (1976) proposed the Finite Strip Method (FSM) to evaluate the buckling ultimate strength of typical thin-walled steel structures. Due to the use of strip elements for discretization, the degrees of freedom of the model are reduced, thereby improving computational efficiency. Lazzari and Batista (2020) involved a computational investigation of the distortional-global buckling interaction behavior of lipped channel sections under pure compression. Adopted the FSM model simplifications to reduce the degrees of freedom in the numerical model led to significant reductions in computational workload and time while maintaining highly alignment with experimental results in the literature. Lazzari and Batista (2021) also presents an FSM-based computational tool for buckling analysis of thin-walled structures, offering a practical and versatile solution applicable to a wide range of crosssectional geometries. These methods improve the calculation speed by reducing the degrees of freedom while ensuring the accuracy of the results, providing important and valuable references for the rapid evaluation of ultimate strength.

Due to the similarity in process between the ISUM and the Smith method, providing the process of the Smith method can help to have a more comprehensive understanding of the ultimate strength assessment of ship hulls. The Smith method was proposed by Smith C.S. (1977) and is an important method for evaluating the ultimate strength of ship hulls. The Smith method assumes that the overall bending moment of the ship is obtained by adding up the bending moments experienced by all elements after discretization. The process of the Smith method is as follows: (i) discretize the ship hull into plate or beam elements (ii) Apply a rotation angle to the neutral axis to all elements (iii) Calculate the strain of the element (iv) Calculate the stress of the element based on the stress-strain relationship of the element (v) The force on the element can be calculated based on the stress and element area (vi) Calculate the bending moment of the element based on the force acting on it and the distance from the neutral axis, and add them together to obtain the bending

moment of the ship under the current turning angle condition repeat the above steps until the turning angle reaches the threshold, and the maximum bending moment value is the ultimate strength of the ship. The limitations of the Smith method can be discovered from the calculation process, which is also a key point of the Smith method. To calculate the ultimate strength of a ship using the Smith method, it is necessary to obtain the stress-strain relationship of the elements.

For the assessment method of ultimate strength under ship fire conditions, based Smith method, Wu et al. (2023) proposed the Fire Smith method to evaluate the ultimate strength of the ship under fire conditions. Wu considered the principle of oxygen consumption and analyzed the impact of the same heat distribution in different areas on the ultimate strength of the ship. Similar to the Smith method, Ueda (2021) first proposed the Ideal Structural Unit Method (ISUM) in 1970s.By modeling large structures as a single large element, this approach leads to fewer elements and improves computational efficiency. The ISUM has been applied in the field of ultimate strength assessment of ship hulls. Paik et al. (2006) et al investigated the ultimate strength of the ship hull of a 120m long aluminum catamaran ship. Based on ISUM, used for progressive collapse analysis of the ship hull. Lindemann et al. (2017) used the ISUM and simulation to research the ultimate strength of box girder under lateral pressure. Gao et al. (2012) used simulation and ISUM to select seven representative crack types for container ships based on the common crack types summarized by the International Association of Classification Societies (IACS), the study analyzed the impact of these cracks on the ultimate strength of the ships. Shi et al. (2012) took container ships as the research object and utilized experiments, nonlinear simulation, and ISUM to study the ultimate strength and failure modes of the hull. Ma et al. (2022) enhanced the ISUM method by incorporating dynamic analysis techniques and applied the improved model to the dynamic ultimate strength assessment of stiffened plates. It can be found that, the Ideal Structural Unit Method (ISUM) has been widely used for evaluating the ultimate strength of ship hulls, but it has hardly been applied in the field of fire safety to date.

By analyzing the research of the above scholars, it has been found that there are currently few full-scale fire tests on ships, which makes it difficult to provide references for other different ship types. Additionally, the finite element method has shortcomings such as a large modeling workload and long calculation times. The main method for theoretically prediction the ultimate strength of ship with fire conditions is proposed by Wu et al. (2023).

However, the Fire Smith method currently uses plate and beam elements to discretize a ship's hull. For large vessels like the USS Bonhomme Richard, a significant number of discrete elements are required, which results in a disadvantage regarding computational speed. In reality, ship fires occur and develop rapidly. Even during the evaluation process, the fire continues to develop, it necessary to evaluate and predict the ultimate strength of the ship hull more quickly. The Fire ISUM can reduce the number of elements, so the Fire ISUM is used to solve the problem of too many elements in the Fire Smith method.

In the Materials and Methods section, we first briefly introduce the advantage of using fewer elements in the Fire ISUM compared to the Fire Smith method, due to the use of stiffened plate element. In section 2.1, the process of the Fire ISUM are proposed. Through the process of using the Fire ISUM, it was found that to evaluating the ultimate strength of ships under fire conditions using Fire ISUM, the key is obtaining the stress-strain relationship of the stiffened plate under elevated temperature conditions. So, in section 2.2, the stress of the stiffened plate under elevated temperature conditions is derived. In section 2.2, it was found that the stress and elastic modulus of stiffened plate are related under the condition of size determination. Therefore, in section 2.3, based on the elastic modulus and the mechanical properties of the stiffened plate under compression under elevated temperature condition. The stress-strain relationship of stiffened plate under elevated temperature conditions was proposed. In Section 2.4, in order to facilitate the understanding and application of fire ISUM, the step-by-step process of the Fire ISUM is presented.

2 Materials and Methods

Before proposing the Fire ISUM, quickly explain its advantages. Figure 3 and 4 compare of Fire Smith method and Fire ISUM for discrete elements of ship hulls. The idea of calculating the ultimate strength of a ship's hull using the Fire Smith method is similar to that of the Fire ISUM, but differs when discretizing elements. The Fire Smith method discretizes the ship's hull into plate and beam elements, while the Fire ISUM discretizes the ship's hull into the largest possible stiffened plate elements. Stiffened plates are composed of multiple plates and beams, so Fire ISUM can effectively reduce the number of elements and improving computational efficiency. From Figures 3 and 4, it can be observed that the Fire ISUM discretizes the ship into stiffened plate elements, which has a lower number of plate and beam elements compared to the Fire Smith method, resulting in higher computational efficiency.

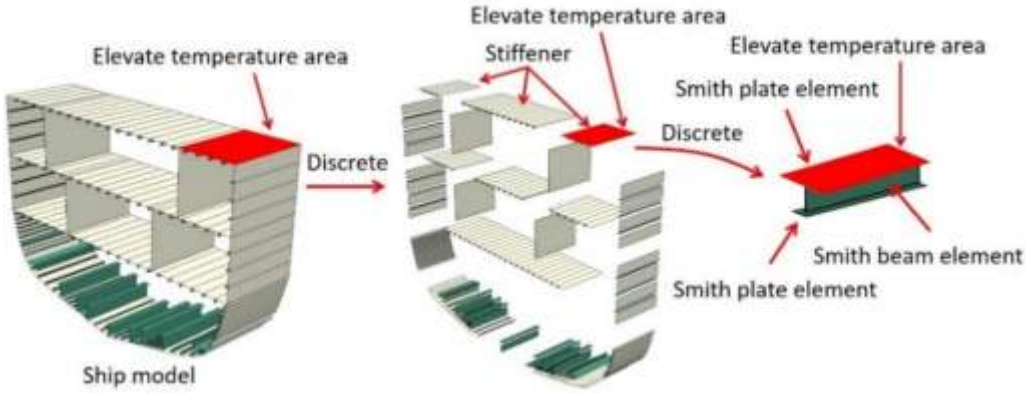

Figure 3: Schematic diagram of ship of Fire Smith method discretization

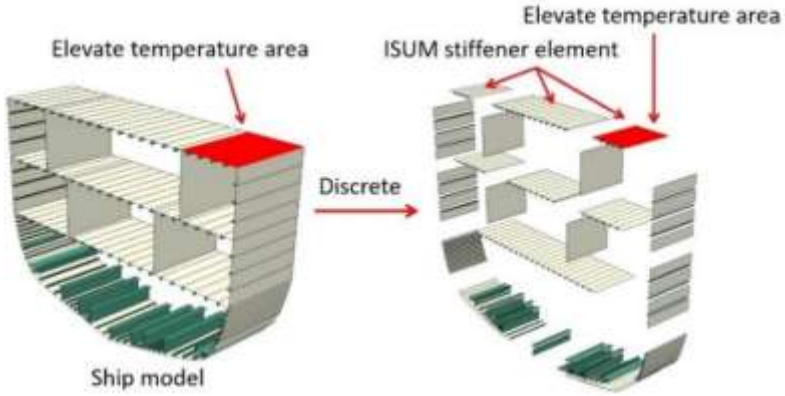

Figure 4: Schematic diagram of ship of Fire ISUM discretization

Figure 5 shows a comparison between the Fire Smith method and the Fire ISUM for the number of elements after discretization. It can be observed that when the number of stiffeners is 1, 5, and 10, the number of elements discretized using the Fire Smith method is 3, 21, and 41, respectively. Fire ISUM discretizes the entire stiffened plate into one stiffened plate element, resulting in a smaller number of elements, and as the number of stiffeners increases, the advantages of the Fire ISUM become more apparent. When the stiffener quantities are 1, 5, and 10 respectively, the number of Fire ISUM elements decreases by 66.7%, 95.2%, and 97.6% compared to the Fire Smith method. From Figure 5, it can be intuitively seen that Fire ISUM has the advantage of discretizing fewer elements for stiffened plates. The reduction in the number of elements results in faster computation speed, thereby improving computational efficiency.

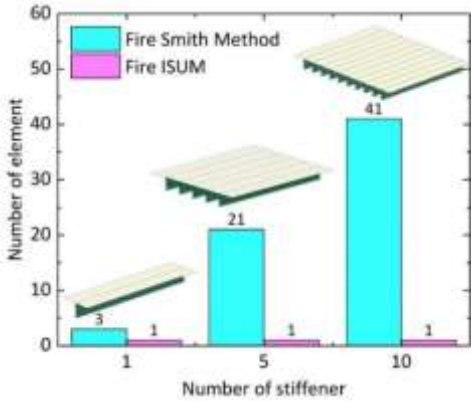

Figure 5: Comparison of Fire Smith method and Fire ISUM for different numbers of stiffener discrete elements

In Figure 6, USNI's LAGRONE (2021) reported an infrared image taken by the US Navy during the fire of the USS Bonhomme Richard. It can be observed that during the ship fire, elevated temperature areas 1 and 2 on the ship's deck show approximately the same distribution. This actual fire case demonstrates the feasibility of simplifying the deck in this area into a stiffened plate element and further illustrates the feasibility of the Fire ISUM.

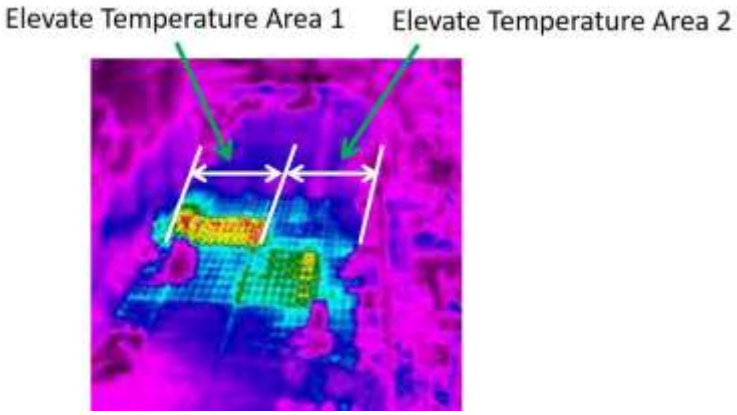

Figure 6: US Fire Pump provided forward-looking infrared (FLIR) imagery of the USS Bonhomme Richard.

2.1 Fire Idealized Structural Unit Method

Based on the strain-stress relationship of the stiffend plate in equation (15). The Fire Idealized Structural Unit Method (ISUM) is proposed, as shown in Figure 7, constructs a temperature matrix based on the temperature field of the fire to be analyzed, assigns unit number *i*, calculates the buckling load under fire conditions, and assumes the buckling strain to obtain stress-strain curves under different temperature conditions, and selects the corresponding curve. Next, based on the input of ISUM elements into the hull structure, the hull structure is discretized into three types of elements: plates, beams, and stiffened plates. Initialize the stress and strain of the ISUM element, construct a deformation matrix, gradually increase rotate angle, and calculate the stiffness matrix changes. Convert the turning angle into structural strain, and determine whether the current buckling load has been reached based on the stress-strain relationship. Once it is reached, the result will be output.

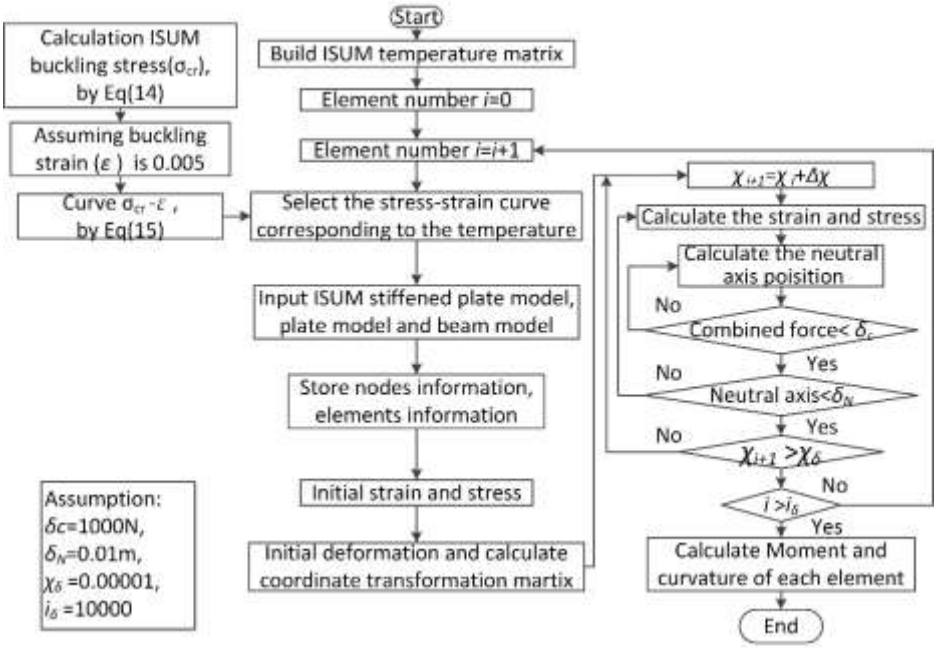

Figure 7: Fire ISUM flowchart

2.2 Critical Buckling Stress

Figure 8 is a forces schematic diagram of the cabin fire. The ship has a width of *L*=12m and a height of *H*=8.1m. It is assumed that the force N_X acting on the ship's deck is a uniformly distributed load, and the boundary conditions are simply supported on all four sides. *a* is the length of the stiffened plate, *B* is the width of the stiffened plate, and *b*/2 is the width of stiffener.

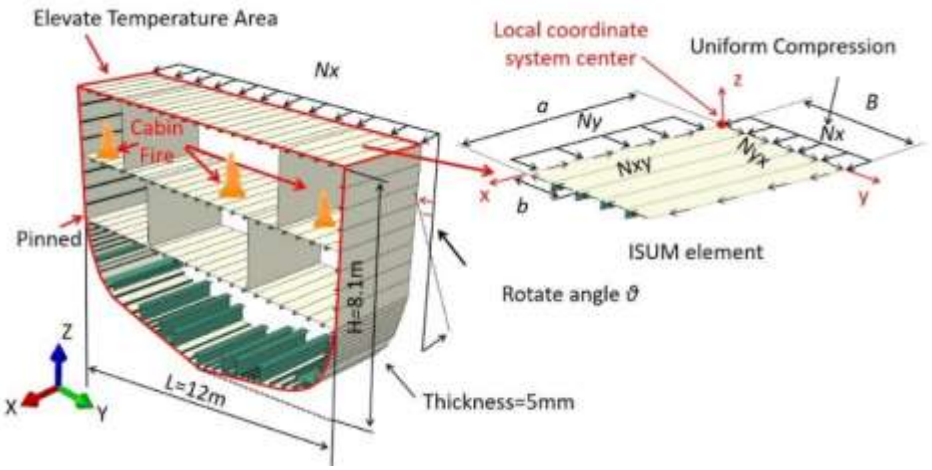

Figure 8: Schematic diagram of stiffened panels in cabin fires

Assumption buckling condition:

$$\omega = \sum_{m=1}^{\infty}\sum_{n=1}^{\infty} A_{mn} \sin\frac{m\pi x}{a}\sin\frac{n\pi y}{b} \tag{1}$$

In a linear system, the expression for the bending strain energy of a plate is shown in equation (2):

$$U = \frac{D}{2}\int\int\left\{\left(\frac{\partial^2\omega}{\partial x^2}+\frac{\partial^2\omega}{\partial y^2}\right)+2(1-\mu)\left[\left(\frac{\partial^2\omega}{\partial x\partial y}-\frac{\partial^2\omega}{\partial x^2}\frac{\partial^2\omega}{\partial y^2}\right)\right]\right\}dxdy \tag{2}$$

The strain energy (ΔU) of bending the plate as equation (3):

$$\Delta U = \frac{D}{2}\int_0^a\int_0^B\left\{\sum_m^\infty\sum_n^\infty A_{mn}\left(\frac{m^2\pi^2}{a^2}+\frac{n^2\pi^2}{B^2}\right)\sin\frac{m\pi x}{a}\sin\frac{n\pi y}{B}\right\}^2 dxdy = \frac{\pi^4 aBD}{8}\sum_m^\infty\sum_n^\infty A_{mn}^2(\frac{m^2}{a^2}+\frac{n^2}{B^2})^2 \tag{3}$$

In equation (3), $D = \frac{Et^3}{12(1-\mu^2)}$.

In local coordinate system, assuming the flexural rigidity of a stiffener (EI) at the distance $c_i=ib/2$ from the edge to y=0, assume that stiffener buckle with plate, the stiffener strain energy as equation (4).

$$\Delta U_i = \frac{EI_i}{2}\int_0^a\left(\frac{\partial^2\omega}{\partial x^2}\right)^2_{y=C_i} dx = \frac{\pi^4 EI}{4a^3}\sum_{m=1}^{\infty} m^4\left(A_{m1}\sin\frac{\pi c_i}{b}+A_{m2}\sin\frac{2\pi c_i}{b}+\cdots\right)^2 \tag{4}$$

In equation (4) i=1,2, ..., N-1.

Assuming that the stiffened plate is only subjected to a force N_x in the X direction, and forces N_y=0 and N_{xy}=0 in other directions. The work energy ΔT as equation (5):

$$\Delta T = \frac{1}{2}\int_0^a\int_0^B\left\{N_x\left(\frac{\partial\omega}{\partial x}\right)^2+N_y\left(\frac{\partial\omega}{\partial y}\right)^2+2N_{xy}\left(\frac{\partial\omega}{\partial x}\frac{\partial\omega}{\partial y}\right)\right\}dxdy = \frac{1}{2}\int_0^a\int_0^B N_x\left(\frac{\partial\omega}{\partial x}\right)^2 dxdy = \frac{N_x aB}{8}\sum_{m=1}^{\infty}\sum_{n=1}^{\infty}A_{mn}^2\frac{m^2\pi^2}{a^2} \tag{5}$$

The work done during buckling by the compressive forces P_i, acting on the plate as equation (6):

$$\Delta T_i = \frac{P_i}{2}\int_0^a\left(\frac{\partial^2\omega}{\partial x^2}\right)_{y=c_i} dx = \frac{P_i}{2}\frac{\pi^2}{a^2}\frac{a}{2}\sum_{m=1}^{\infty} m^2(A_{m1}\sin\frac{\pi c_i}{b}+A_{m2}\sin\frac{2\pi c_i}{b}+\cdots)^2 \tag{6}$$

According to Timoshenko's energy method theory, when the external force on the stiffened plate exceeds the strain energy, the stiffened plate is considered to be in an unstable state. Therefore, the buckling load of the stiffened plate can be determined by equating the strain energy to the work done by the external forces, calculated using equation (7).

$$\Delta U + \Delta\sum_{i=1}^{n-1}U_i = \Delta T + \Delta\sum_{i=1}^{n-1}T_i \tag{7}$$

Assuming the following parameters as equation (8):

$$\beta = \frac{a}{B}, \gamma_i = \frac{EI_i}{BD}, \delta_i = \frac{P_i}{BN_x} = \frac{A_i}{Bt} \tag{8}$$

In equation (8), β is the aspect ratio of the stiffened plate, γ_i is the ratio of the bending stiffness of the stiffeners to that of the plate, and δ_i is the ratio of the cross-sectional area of the stiffeners to that of the plate. I_i and A_i are the moment of inertia and the cross-sectional area of the stiffener, respectively.

Bringing equation (3), (4), (5), (6) into (7), to calculate the σ_{cr} as equation (9).

$$\sigma_{cr} = \frac{\pi^2 D}{B^2 t \beta^2} \frac{\sum_{m=1}^{\infty}\sum_{n=1}^{\infty} A_{mn}^2 (m^2 + n^2\pi^2)^2 + 2\sum_{i=1}^{N-1}\gamma_i \sum_{m=1}^{\infty} m^4 \left(\sum_{n=1}^{\infty} A_{mn} \sin\frac{n\pi c_i}{b}\right)^2}{\sum_{m=1}^{\infty}\sum_{n=1}^{\infty} m^2 A_{mn}^2 + 2\sum_{i=1}^{N-1}\delta_i \sum_{m=1}^{\infty} m^2 \left(\sum_{n=1}^{\infty} A_{mn} \sin\frac{n\pi c_i}{b}\right)^2} \tag{9}$$

Calculate the derivative of A_{mn} for equation (9) and set equation (10) equal to 0.

$$\frac{\pi^2 D}{B^2 t}(A_{mn}(m^2 + n^2\pi^2)^2 + 2\sum_{i=1}^{N-1}\gamma_i \sin\frac{ni\pi}{N} m^4 \sum_{p=1}^{\infty} A_{mp} \sin\frac{p\pi c_i}{b}) - \beta^2\sigma_{cr}\left(m^2 A_{mn} + 2\sum_{i=1}^{N-1}\delta_i \sin\frac{n\pi c_i}{b} m^2 \sum_{i=1}^{\infty} A_{mp} \sin\frac{p\pi c_i}{b}\right) = 0 \tag{10}$$

By equating to zero the determinant of this system of equations, it can obtain an equation for determining σ_{cr}. As shown in (11).

$$\sigma_{cr} = \frac{\pi^2 D}{B^2 t} \frac{(1+\beta^2)^2 + 2\gamma}{\beta^2(1+2\delta)} \tag{11}$$

For multiple stiffeners, the buckling stress of the stiffened plate can be determined using equation (10), as shown in equation (12):

$$\sigma_{cr} = \frac{\pi^2}{B^2 t} \frac{Et^3}{12(1-\mu^2)} \frac{(1+\beta^2)^2 + (n+1)\gamma}{\beta^2(1+(n+1)\delta)} \tag{12}$$

It can be found from equation (12), under the condition of determining the size of the stiffened plate, the buckling stress and elastic modulus are related.

2.3 Mechanical Properties at Elevated Temperatures

In section 2.2, the relationship between the ultimate strength and elastic modulus of stiffened plates is established. High temperatures lead to a decrease in the elastic modulus of stiffened plates, so the relationship between temperature and elastic modulus is analyzed in section 2.3.

The ship material in Figure 8 is H36 steel, with an elastic modulus of 206GPa and Poisson's ratio of 0.3 at 20 °C. The variation of H36 steel under elevated temperature conditions is shown in Figure 9. The elastic modulus parameter proposed by the American Steel Structure Code Committee (AISC) (2005) in 2005 fits the elastic modulus with elevated temperature conditions according to these data. The temperature curve of elastic modulus was fitted using the Langevin Mod exponential function, with an R^2 of 0.99. For the fitting function of elastic modulus under elevate temperature conditions, refer to the table on the right side of Figure 9.

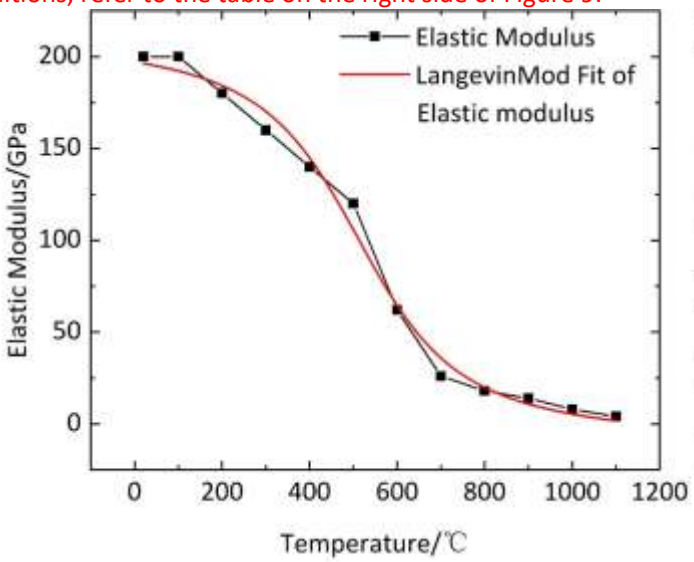

Model	LangevinMod

Equation	double z=(x-xc)/s;
	double cothz=cosh(z)/sinh(z);
	y=y0+ C * (cothz-1/z);

Plot	Elastic modulus
y0	100.80829 ± 3.89505
xc	511.33149 ± 18.16414
C	116.82488 ± 8.33826
s	-89.61256 ± 16.58991
Reduced Chi-Sqr	69.26785
R-Square (COD)	0.99212
Adj. R-square	0.98917

Figure 9: Elastic modulus and linear fitting curve of H36 steel

Drawing from the graph of elastic modulus data, it is possible to formulate as equation (13) that describes the elastic modulus at elevated temperatures.

$$E_T = 100.8 + 116.8\left(\coth\left(\frac{T-511.3}{-89.6}\right) + \frac{89.6}{T-511.3}\right), 0 \le T \le 1200 \quad (13)$$

After determining the elastic modulus of the material at different temperatures, the ultimate strength of the stiffened plate at different temperatures is determined. However, further determination of the stress-strain relationship is needed, and the stress-strain characteristics of the stiffend plate will be determined through high-temperature testing.

The study of the mechanical properties of steel structures at high temperatures has been continuously explored in the field of structural engineering, yielding significant references over the years. Sánchez Cruz et al. (2015) investigated steel-concrete composite beams with fire-resistant coatings under axial and rotational constraints, highlighting the importance of considering the interaction forces between beams and columns in design processes. Moving forward, Al-Rousan et al. (2021) analyzed the behavior of rectangular reinforced concrete (RC) columns reinforced with auxetic steel mesh at high temperatures. His research involved testing 24 rectangular RC column specimens with a 1/3 scale ratio under axial loading to evaluate how different layers of auxetic steel mesh perform when exposed to elevated temperatures. More recently, in 2023, Leite et al. (2023) focused on the performance of steel-concrete composite beams with fire-resistant coatings under axial and rotational constraints. He studied axial forces across different spans, under both constraints, and analyzed four different fire-resistant coating materials in fire conditions.

For the mechanical properties of stiffened plates under elevated temperature conditions, previous studies have provided important references. The research on the mechanical properties of stiffened plates under high temperature conditions by scholars also serves as an important reference. Tan et al. (2008) conducted compression buckling tests on stiffened plates at three temperatures: 400°C, 550°C, and 670°C. Figure 10 shows a schematic diagram of the compression test for stiffened plates at 670°C. Tan measured the force and displacement curves at different temperatures, as shown in Figure 11, providing a reference for the study of the mechanical properties of stiffened plates under fire conditions.

Figure 10: Tan et al. (2008) stiffened plate test with high temperature

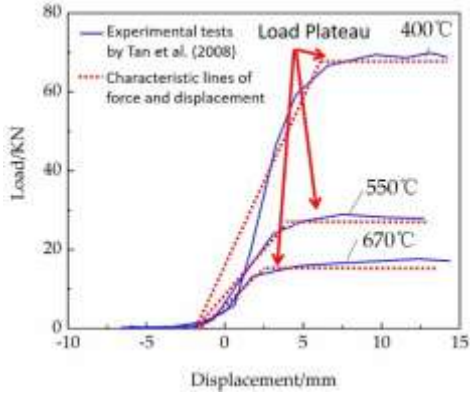

Figure 11: Tan et al. (2008) measured the high-temperature force displacement curve of the stiffened plate

Wang et al. (2020) conducted a buckling strength test on T-shaped stiffened plates under different temperature conditions ranging from 20 to 800°C. Figure 12 shows the failure mode of compression buckling for T-shaped stiffened plates in Wang's test. As shown in Figure 13, as the temperature increased, the ultimate strength of the T-shaped stiffened plates gradually decreased. At a certain temperature condition, when the ultimate strength reaches its maximum value, the force does not increase with the displacement in some ranges. This phenomenon is referred to as the “Load Plateau” Furthermore, the higher the temperature, the longer the “Load Plateau”.

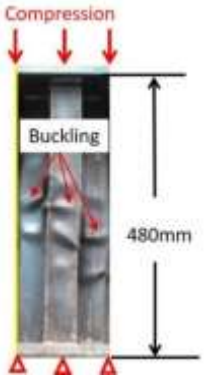

Figure 12: Wang et al. (2020) buckling test of stiffened plates high temperature

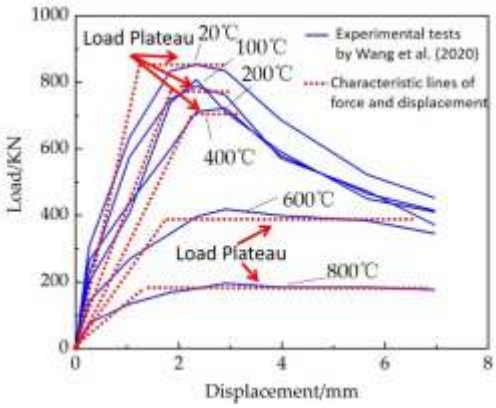

Figure 13: Wang et al. (2020) measured the force and displacement curves of T-shaped stiffened plates under high temperature conditions

Based on equation (12) and (13), equation (14) for calculating the ultimate strength of stiffened plates under fire conditions is proposed.

$$\sigma_{cr}=\left(\frac{\pi^2}{b^2t}\frac{t^3}{12\left(1-\mu^2\right)}\frac{\left(1+\beta^2\right)+(\mathrm{n}+1)\gamma}{\beta^2\left(1+(n+1)\delta\right)}\right)\left(100.8+116.8\left(\coth\left(\frac{T-511.3}{-89.6}\right)+\frac{89.6}{T-511.3}\right)\right) \tag{14}$$

According to the force and displacement characteristics of stiffened plates under elevated temperature conditions in Wang et al. (2020) literature, we assume from equation (14) that there is approximately linear stress-strain behavior before reaching the buckling strength. For an elastic strain of 0.005, based on Wang et al. experiment, the total length of the stiffened plate is 480 mm, and the deformation at buckling is about 2 mm. The deformation is calculated as 2 mm divided by the total length, resulting in 2/480 = 0.00416, which supports the assumption that the elastic strain is 0.005. In addition, when calculating a very small strain (Δε) after reaching the maximum stress, a constant stress should be maintained.

$$\sigma_{\mathrm{x}}=\begin{cases}\dfrac{\sigma_{\mathrm{cr}}}{0.005}\varepsilon & 0<\varepsilon<0.005\\ \sigma_{\mathrm{cr}} & 0.005\le\varepsilon<\varepsilon+\Delta\varepsilon\end{cases} \tag{15}$$

2.4 Step-by-step Procedure

The Step-by-step procedure of Fire ISUM in Figure 14 is as follows:

· Step 1, build a temperature matrix.

· Step 2, discretize the ship into stiffened plates of cabin length, compared with plate and beam elements, the number of reinforced plate elements is reduced, and the calculation speed is faster, thereby improving the calculation efficiency.

· Step 3, gradually increase the curvature of the hull bending for loading.

· Step 4, calculate the element strain according to the rotation angle.

· Step 5, calculate the stress according to the corresponding temperature's stress-strain relationship of the element after obtaining the strain.

· Step 6, calculate the force of each element according to stress and element area, and then calculate the moment of each element.

· Step 7, obtain the bending moment-curvature curve of the entire hull structure, and the corresponding ultimate bending moment, i.e., the ultimate strength value of the hull, is obtained.

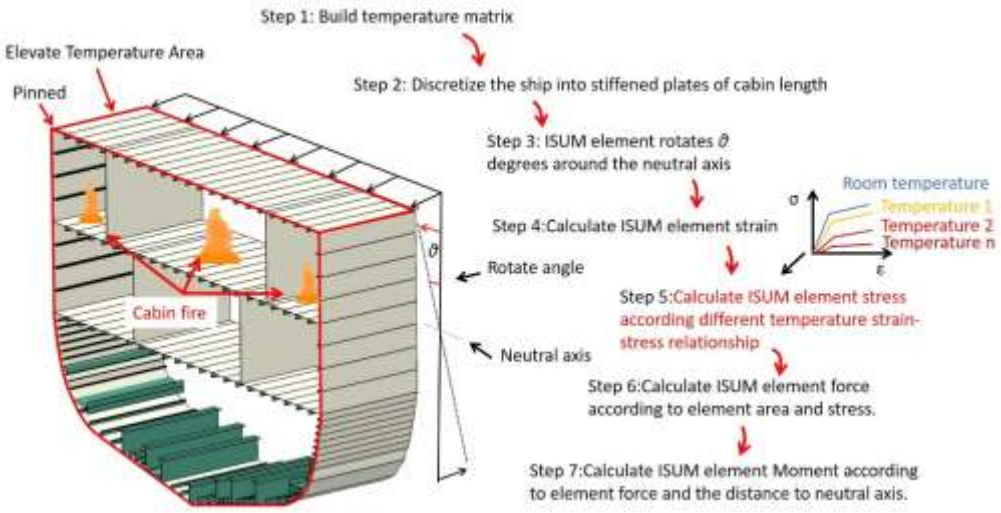

Figure 14: Schematic diagram of the calculation process of Fire Idealized Structural Unit Method (ISUM)

3 Simulation Setup

To verify the effectiveness of the Fire ISUM and study the ultimate strength characteristics of cabin fires at different locations, calculations were performed for cabin fires at four locations. Abaqus is used for simulation calculation, assume a bilinear material model with no strain hardening, the elastic modulus of the material is 210GPa, Poisson's ratio is 0.3, and yield strength is 355MPa. For residual stress, C. Guedes Soares et al. (2008) studied the effect of different residual stresses on the ultimate strength of ships. Regarding hogging condition, the error when considering versus not considering residual stress was 1.89%, while for sagging condition, the error was 6.1%. Mei et al. (2021) simultaneously considered the effects of residual stress and varying degrees of initial imperfection on the ultimate strength of ships and found that the larger the initial imperfection amplitude of the structure, the smaller the impact of welding residual stress on the ultimate strength of the stiffened plate. According to the above research, residual stress has a relatively small impact on ultimate strength than elevate temperature condition, and the greater the deformation of the ship, the smaller the impact of residual stress on ultimate strength. Therefore, the influence of residual stress is therefore not considered in this study. As depicted in Figure 15, it was assumed that the high-temperature areas in each cabin were evenly distributed during the fire, with temperatures ranging from 100°C to 1200°C. Specifically, Figure 15(a) shows an elevated temperature area with a width of W_1=2.2m, Figure 15(b) shows a width of W_2=3.3m, Figure 15(c) shows a width of W_3=4.4m, and Figure 15(d) shows a width of W_4 = 6.6m. Table 2 details the working conditions for various cabin temperatures and elevated temperature area widths.

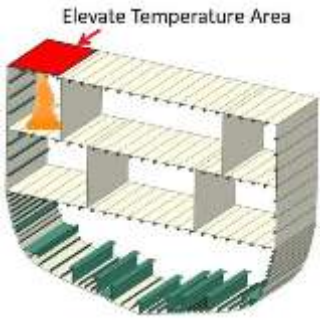

(a)Elevate temperature area W_1 = 2.2 m

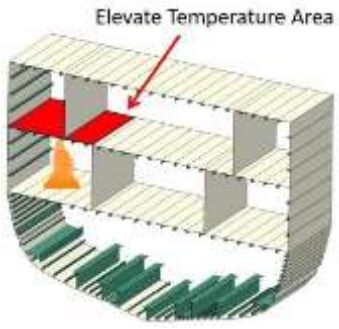

(b)Elevate temperature area W_2 = 3.3 m

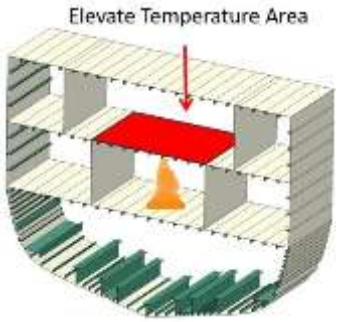

(c)Elevate temperature area W_3 = 4.4 m

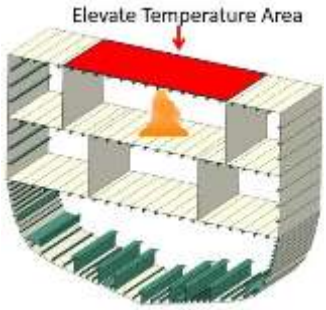

(d)Elevate temperature area W_4 = 6.6 m

Figure 15: Schematic diagram of fires in different compartments

Table 2 Working condition table.

No.	$T_1 \times W_1$	$T_2 \times W_2$	$T_3 \times W_3$	$T_4 \times W_4$
1	100 × 2.2	100 × 3.3	100 × 4.4	100 × 6.6
2	200 × 2.2	200 × 3.3	200 × 4.4	200 × 6.6
3	300 × 2.2	300 × 3.3	300 × 4.4	300 × 6.6
4	400 × 2.2	400 × 3.3	400 × 4.4	400 × 6.6
5	500 × 2.2	500 × 3.3	500 × 4.4	500 × 6.6
6	600 × 2.2	600 × 3.3	600 × 4.4	600 × 6.6
7	700 × 2.2	700 × 3.3	700 × 4.4	700 × 6.6
8	800 × 2.2	800 × 3.3	800 × 4.4	800 × 6.6
9	900 × 2.2	900 × 3.3	900 × 4.4	900 × 6.6
10	1000 × 2.2	1000 × 3.3	1000 × 4.4	1000 × 6.6
11	1100 × 2.2	1100 × 3.3	1100 × 4.4	1100 × 6.6
12	1200 × 2.2	1200 × 3.3	1200 × 4.4	1200 × 6.6

The initial imperfection in the stiffened plates are caused by manufacturing. This article considers the initial imperfection of the ship in the simulation, assuming that the current deformation is due to the average imperfection conditions provided by Smith (1975). Different welding processes can be categorized into three levels of imperfection, as shown in equation (16). Here, an average imperfection level of ω_p =0.1 $\beta^2 t$ is selected, where β (as shown in equation (16)) represents the plate flexibility, and t represents the plate thickness.

$$\omega_p = \begin{cases} 0.025\beta^2 t & \text{for slight imperfection} \\ 0.1\beta^2 t & \text{for average imperfection} \\ 0.3\beta^2 t & \text{for severe imperfection} \end{cases} \tag{16}$$

In equation (16), $\beta = \frac{b}{t}\sqrt{\frac{\sigma_y}{E}}$,σ_y represents the yield strength of H36 steel, which is 355 MPa, and E denotes the elastic modulus, equal to 210 GPa.

The determination of the ship's ultimate strength at high temperatures is carried out through a two-stage process: the first stage involves thermal mechanical coupling calculations, and the second stage involves explicit dynamic calculations. The boundary conditions are defined as shown in Figure 16. Elevate temperature area are applied above the deck with pinned boundary conditions at both ends.

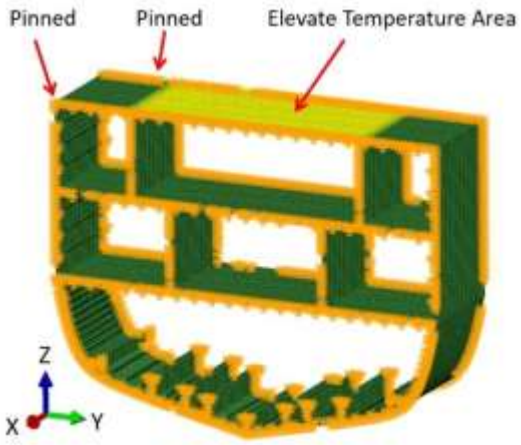

Figure 16: Boundary condition for ship model thermal-mechanical coupling simulation

For the explicit dynamic calculation stage, use predefined field methods defined the elevate temperature field to the deck; the boundary conditions are shown in Figure 17. The element type is S4RT. The hull was simply supported, while the other end was constrained in Y and Z directional movements and rotations in the X and Z directions. Rotate the entire plane by 0.2 degrees around the Y axis. The moment value represented the ultimate high-temperature strength.

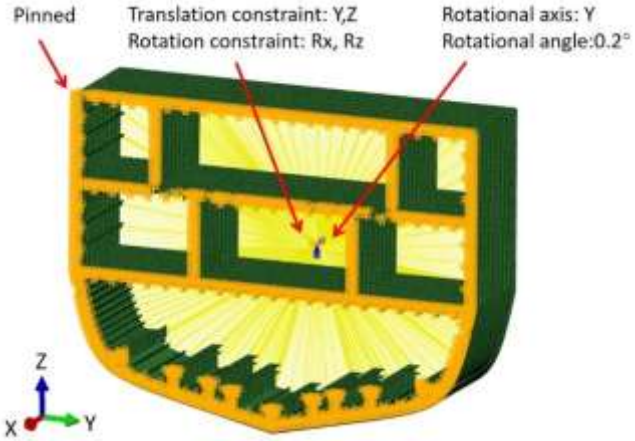

Figure 17: Boundary conditions for ship model explicit dynamic simulation

4 Mesh Sensitivity Analysis

The mesh has an impact on the results of finite element simulation. Under normal circumstances, the more meshes there are, the more the results tend to converge. However, it is also important to note that the calculation time should not be too long. Therefore, it is necessary to confirm the number of meshes and the accuracy of the calculation results. To prove the mesh sensitivity on the ultimate strength of the ship, the total number of meshes for mesh sizes of 0.2m, 0.15m, 0.1m, 0.075m, and 0.05m were 11,610, 16,740, 35,960, 60,480, and 119,760, respectively. As shown in Figure 18, the ultimate strength of ship with multiple mesh sizes was simulation. Result show that the ultimate strength decreased as the number of meshes increased. The ultimate strengths for multiple meshes were 3.571×10^8 N·m, 3.113×10^8 N·m, 2.726×10^8 N·m, 2.678×10^8 N·m and 2.672×10^8 N·m, respectively.

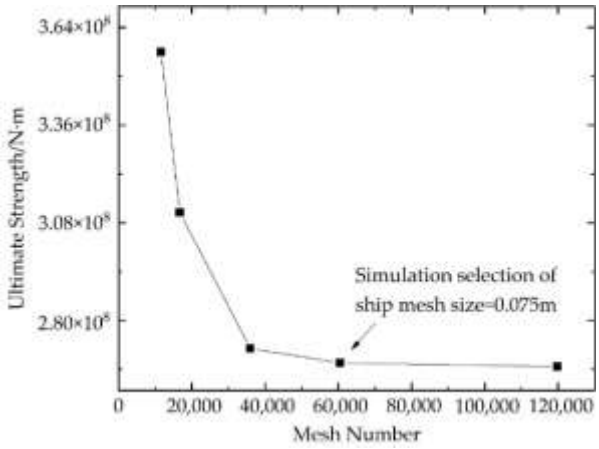

Figure 18: Relationship between mesh size and ultimate strength of vessel

The calculation results consider both calculation speed and accuracy. The ship's mesh is displayed in Figure 19, There is an overall and specific detail pictures. The mesh size of the ship is 0.075 m, featuring a quadrilateral mesh type with a number of 60,480 elements.

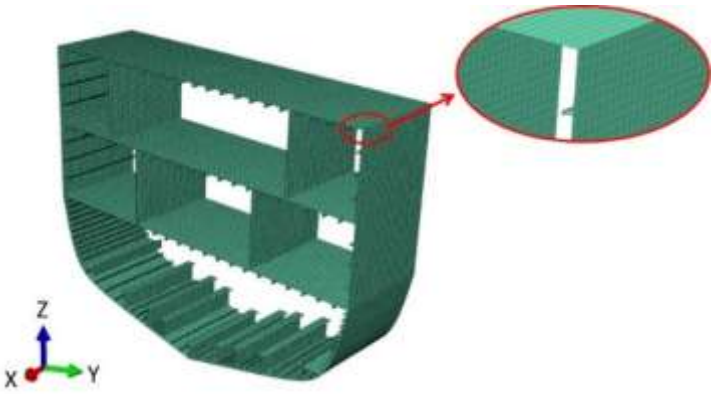

Figure 19: Mesh diagram of overall and specific detail

5 Results

To verify the feasibility of the critical buckling stress equation (15), the stiffened plate in the elevated temperature area 1 was analysed. The results of equation (15) and ABAQUS were compared under normal temperature conditions. The critical stress from the simulation was 191 MPa, while equation (15) yielded 180 MPa, with an error of about 5.6%.

Figure 20 displays the deformation of the hull under the combined influence of initial imperfection and high temperature. Overall, the deformation from initial imperfection at different locations tends to increase gradually as the temperature rises. The deformation characteristics shown in Figures 20(a) to 20(d) are described as 'wavy', which exacerbates the influence of initial imperfection on the ultimate strength of the ship. In other words, in addition to the weakening of the material's mechanical properties due to temperature rise, the combined effects of initial imperfection and elevated temperatures also significantly influence the structural deformation and ultimately affect the ship's strength. Comparing different elevated temperature areas, it is evident that as the area exposed to elevated temperatures increases, the stiffness of the ship's deck decreases, and the deformation correspondingly intensifies.

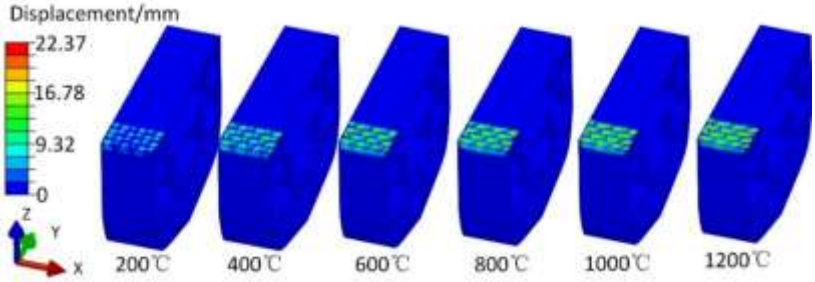

(a) Deformation with elevated temperature in working condition 1.

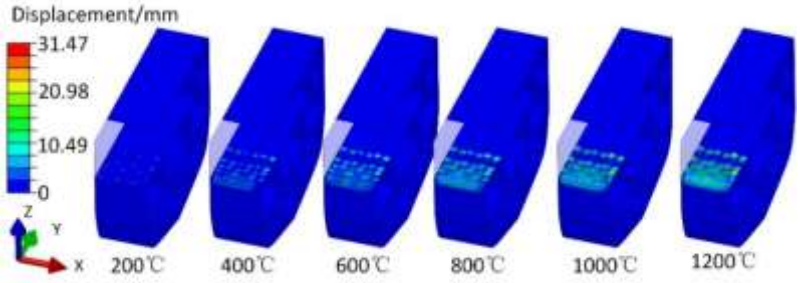

(b) Deformation with elevated temperature in working condition 2.

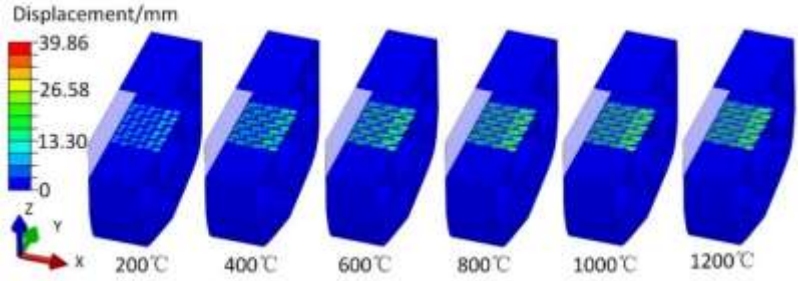

(c) Deformation with elevated temperature in working condition 3.

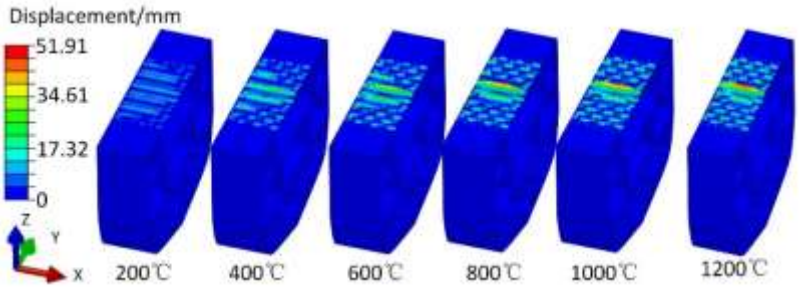

(d) Deformation with elevated temperature in working condition 4.

Figure 20: Hull deformation under elevate temperature and initial imperfection effects

Figure 21 represents the ultimate strength at different elevated temperature areas and temperatures. Figures 21(a) - 21(d) represent elevated temperature areas of 2.2m, 3.3m, 4.4m, and 6.6m, respectively. Overall, under the conditions of elevated temperature areas and temperatures, the ultimate strength rapidly reaches its maximum value with the increase of the rotation angle, and then slowly decays after reaching this peak. This peak value represents the ultimate strength corresponding to the current elevated temperature area and temperature of the ship. When comparing the four different elevated temperature areas, it can be observed that the ultimate strength of the ship decreases in all areas as the temperature increases, indicating a decrease in the ship's ultimate strength with an increase in temperature.

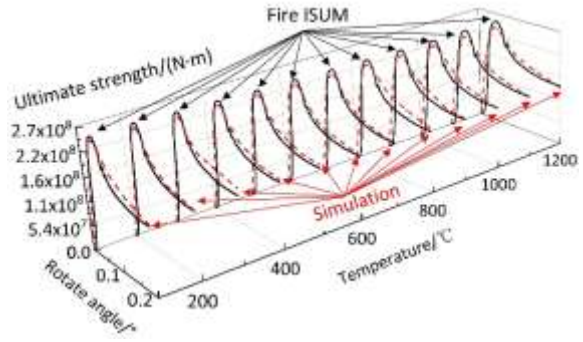

(a) Elevate temperature area W_1 = 2.2 m

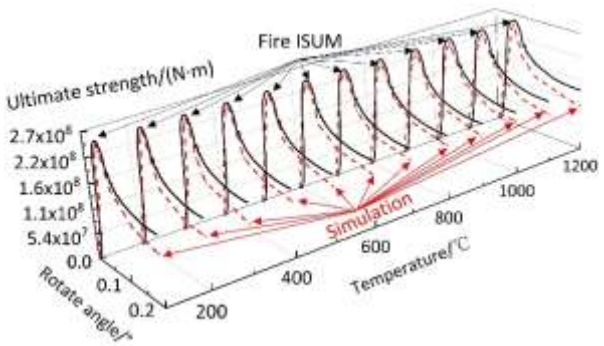

(b) Elevate temperature area W_2 = 3.3 m

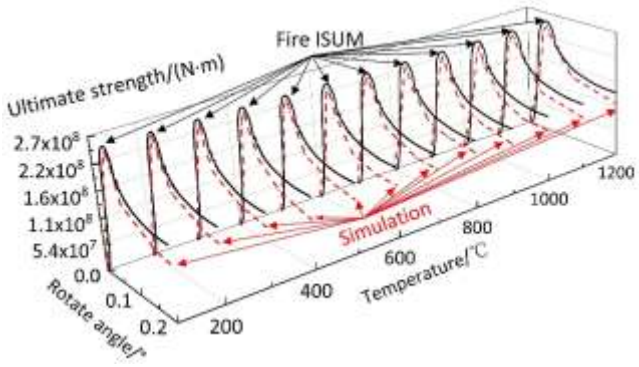

(c) Elevate temperature area W_3 = 4.4 m

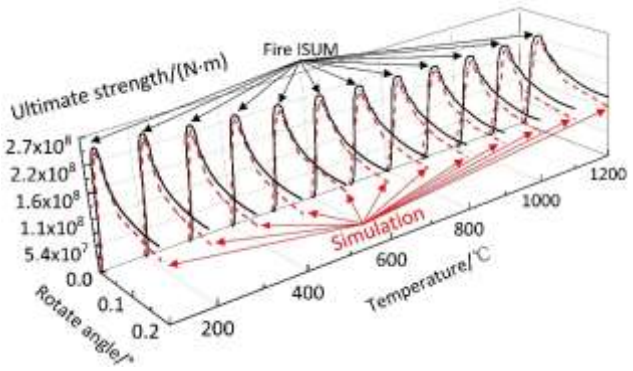

(d) Elevate temperature area W_4 = 6.6 m

Figure 21: Comparison of Fire ISUM and simulation result for ship ultimate strength.

In order to further analyze the influence of high temperature and initial imperfection on the ultimate strength of the ship, the ultimate strength values for different regions and temperatures shown in Figure 21 were extracted and compared using the Fire ISUM method. As observed from Figure 22 and Table 3, both the simulation results and the Fire ISUM comparisons show that the ultimate strength of the ship gradually decreases with increasing temperature. The consistent trends between these two methods indicate that the Fire ISUM is capable of calculating the impact of high temperature on the ultimate strength of the ship.

When comparing the ultimate strength at the same temperature and different elevate temperature area, it can be found that the simulation results are smaller than those obtained using the Fire ISUM. This discrepancy occurs because the simulation considers the influence of initial imperfection on the ultimate strength of the ship, which the Fire ISUM method currently does not account for. Table 3 presents the results from both the simulation and the Fire ISUM at various temperatures, and also provides the differences between the two. Comparing simulations at increasing temperatures with the Fire ISUM results, it was observed that as the simulation temperature rose, initial imperfection led to more significant deformation, resulting in final simulation values that were smaller than those calculated by the Fire ISUM. Moreover, as the temperature increased, the discrepancies also grew, reaching a maximum error of 5.24%. Although the error between simulation and the Fire ISUM method increases with the increase of temperature, the material may melt and be unable to bear external forces when the temperature further increases. Therefore, the Fire ISUM method covers the temperature range at which the ship deck can withstand external forces when a fire occurs and has the potential to be used as a method for evaluating the ultimate strength of ship fires.

When the elevated temperature area is located on different decks, the larger the elevated temperature area, the greater the decrease in ultimate strength. For example, in the elevated temperature area W_1=2.2m on the first deck, the ultimate strength decreases by 8.93%. Similarly, in the elevated temperature area W_4=6.6m on the first deck, the ultimate strength of the ship decreases by 18.77%. In cases where the elevated temperature areas are on the second deck, the ultimate strength decreases by 6.15% at W_2=3.3m and by 8.1% at W_3=4.4m. It can be noted that, the decrease in ultimate strength in the 2.2m heating area was more significant than in the 3.3m and 4.4m heating areas. The decrease in ultimate

strength caused by high temperatures in a fire is not only related to the width of the elevated temperature area but also the distance between deck and neutral axis. The elevate temperature areas of 2.2m and 6.6m are on the same deck, with a distance of 4.2m from the neutral axis. The elevate temperature areas of 3.3m and 6.6m are on the same deck, with a distance of 1.8m from the neutral axis. The width of the elevate temperature areas is 6.6m, which is larger than other elevate temperature areas, and its distance from the neutral axis is greater, so the ultimate strength decreases more. For the 2.2m elevate temperature areas, although it is smaller than the 3.3m and 4.4m, its distance from the neutral axis is greater, resulting in a greater decrease in ultimate strength.

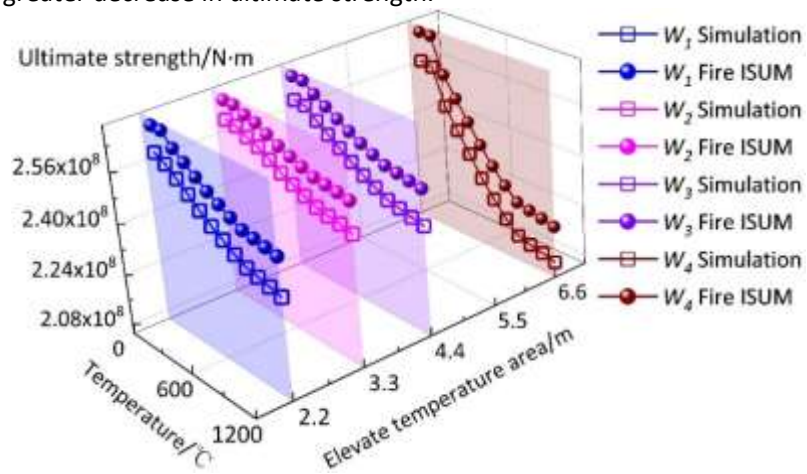

Figure 22: Ultimate strength with Fire ISUM and simulation in different elevate temperature areas and temperatures.

Table 3 Ultimate strength value and error of simulation and Fire ISUM.

No.	W_1 = 2.2 m			W_2 = 3.3 m		
	FEM/(N·m)	Fire ISUM/(N·m)	Error (%)	FEM/(N·m)	Fire ISUM/(N·m)	Error (%)
1	2.596×10^8	2.678×10^8	3.06	2.618×10^8	2.678×10^8	2.25
2	2.577×10^8	2.678×10^8	3.22	2.613×10^8	2.678×10^8	2.41
3	2.549×10^8	2.640×10^8	3.43	2.595×10^8	2.662×10^8	2.53
4	2.519×10^8	2.614×10^8	3.62	2.581×10^8	2.653×10^8	2.71
5	2.488×10^8	2.587×10^8	3.83	2.558×10^8	2.634×10^8	2.90
6	2.459×10^8	2.562×10^8	4.01	2.534×10^8	2.615×10^8	3.08
7	2.436×10^8	2.541×10^8	4.12	2.516×10^8	2.599×10^8	3.18
8	2.411×10^8	2.520×10^8	4.31	2.499×10^8	2.585×10^8	3.31
9	2.391×10^8	2.502×10^8	4.43	2.482×10^8	2.571×10^8	3.46
10	2.383×10^8	2.496×10^8	4.52	2.474×10^8	2.566×10^8	3.57
11	2.374×10^8	2.489×10^8	4.64	2.468×10^8	2.561×10^8	3.64
12	2.364×10^8	2.482×10^8	4.75	2.457×10^8	2.554×10^8	3.78
No.	**W_3 =4.4m**			**W_4 = 6.6 m**		
	FEM /(N·m)	**Fire ISUM/(N·m)**	**Error (%)**	**FEM /(N·m)**	**Fire ISUM/(N·m)**	**Error (%)**
1	2.604×10^8	2.678×10^8	2.77	2.584×10^8	2.678×10^8	3.52
2	2.600×10^8	2.678×10^8	2.91	2.577×10^8	2.678×10^8	3.76
3	2.568×10^8	2.650×10^8	3.10	2.463×10^8	2.565×10^8	3.97
4	2.540×10^8	2.626×10^8	3.29	2.398×10^8	2.502×10^8	4.14
5	2.513×10^8	2.603×10^8	3.46	2.335×10^8	2.440×10^8	4.32
6	2.486×10^8	2.580×10^8	3.64	2.271×10^8	2.380×10^8	4.59
7	2.461×10^8	2.559×10^8	3.82	2.217×10^8	2.327×10^8	4.71
8	2.440×10^8	2.541×10^8	3.98	2.169×10^8	2.280×10^8	4.85
9	2.419×10^8	2.524×10^8	4.15	2.131×10^8	2.242×10^8	4.97
10	2.411×10^8	2.518×10^8	4.26	2.119×10^8	2.232×10^8	5.07
11	2.401×10^8	2.511×10^8	4.37	2.110×10^8	2.224×10^8	5.12
12	2.393×10^8	2.505×10^8	4.48	2.099×10^8	2.215×10^8	5.24

To study the factors affecting the attenuation of ultimate strength under elevate temperature conditions, the attenuation factor for ultimate strength is defined as I_{URi}, where I_{URi}=1-(M_i/M). Here, 'M_i' represents the ultimate strength

at different temperatures, and '*M*' represents the ultimate strength at room temperature. Figure 23 displays the ratio of the ultimate strength attenuation factor I_{UR} to the width of each compartment. By analyzing the relationship between the compartment widths and the ultimate strengths under working conditions 1-4, it is observed that the ultimate strengths under working conditions 1, 2, and those under 3, 4 are grouped into two distinct categories after accounting for the width of the high-temperature area. Furthermore, the distances from the neutral axis to the high temperature regions are identical for workingconditions 1, 2, and for 3, 4. Dividing the data by the distance from the neutral axis, as shown in Figure 24, reveals that the differences in ultimate strength between boundary conditions 1-4 are not significant. Therefore, it can be concluded that the ultimate strength under high temperature conditions is correlated with the distance between the high temperature region and the neutral axis.

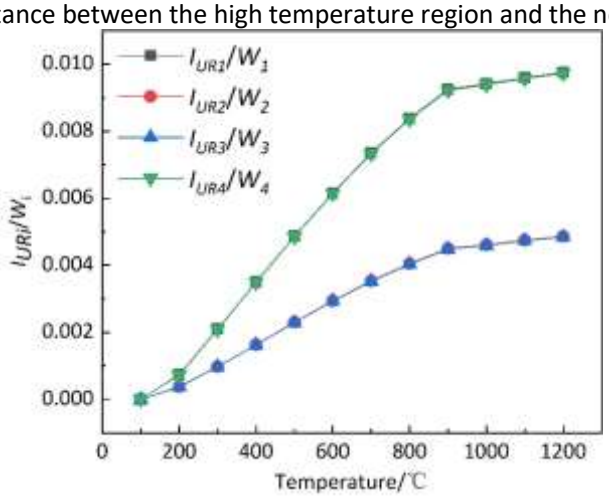

Figure 23: I_{URi}/W_i under elevate temperature conditions

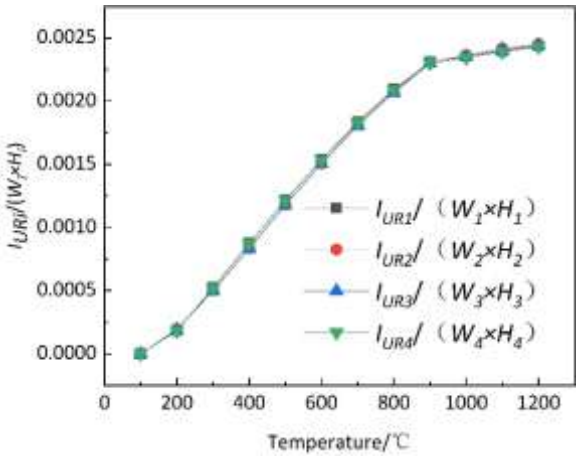

Figure 24: $I_{URi}/(W_i \times H_i)$ under elevate temperature conditions

6 Conclusions

To evaluate and prediction the ultimate strength of ships under ship fire conditions more quickly, the Fire ISUM is proposed. Based on the force and displacement characteristic measured in the stiffened plate fire test, the stress-strain relationship of the stiffened plate under fire conditions was proposed. Compared to Fire Smith method, Fire ISUM has fewer elements and can evaluate the ultimate strength of the ship under fire conditions more quickly.

Through simulations and Fire ISUM calculations of the ultimate strength of compartments with different elevated temperature conditions, it has been found that the trends in the simulation results and Fire ISUM results are similar. However, due to the initial imperfections in the ship used for the simulations, the values obtained from the simulations are smaller than those from the Fire ISUM.

Through calculation, it was determined that high temperature is not the only factor affecting the attenuation of ultimate strength. Therefore, to study the factors influencing the ultimate strength of ships under high temperature conditions, the ultimate strength attenuation factor, I_{UR}, was defined. This factor was used to relate the width of the elevated temperature area to the distance from the neutral axis. It was found that the proportion of the ultimate strength attenuation factor remained consistent when the width and the distance from the neutral axis were the same. This indicates that the main factors affecting ultimate strength attenuation under fire conditions are the width of the elevated temperature area and the distance from the neutral axis.

At present, there are still limitations in the Fire ISUM. The assumed buckling deformation conditions used in the Fire ISUM cannot consider the influence of initial imperfections. In the future, theoretical and experimental research on the buckling strength of stiffened plates under initial imperfection conditions should be further improved. Currently, the element characteristics of the Fire ISUM are based on small-scale experiments. In the future, more ultimate strength tests should be conducted under ship fire conditions to correct the element characteristics of Fire ISUM and improve its accuracy. Additionally, Fire ISUM can be applied to ships with multiple decks to assess the impact of fires on large vessels. Currently, the temperature matrix of Fire ISUM directly defines temperature; in the future, fire temperature field algorithms can also be developed to better relate Fire ISUM to the impact of real fires

Author's Contribuitions: Conceptualization, J.X Wu. and M. Yan; Methodology, J.X Wu; Investigation, J.X Wu; Writing - original draft, J.X Wu; Writing - review & editing, J.X Wu; Funding acquisition, M. Yan and X.W. Sun; Resources, M. Yan; Supervision, M. Yan and X.W. Sun.

Editor: Rogério José Marczak

References

Al-Rousan, R. Z., (2021). Behavior of auxetic steel wire RC columns exposed to elevated temperature. Latin American Journal of Solids and Structures 18(02), e351, doi:10.1590/1679-78256422.

Baalisampang, T., Abbassi, R., Garaniya, V., Khan, F., Dadashzadeh, M., (2018). Review and analysis of fire and explosion accide nts in maritime transportation. Ocean Engineering 158:350-366, doi.org/10.1016/j.oceaneng.2018.04.022.

Barichello, C., Landesmann, A., & Camotim, D., (2017). Distortional Failure and DSM Design of Cold-Formed Steel S-Shaped Bea ms Under Uniform Bending.Latin American Journal of Solids and Structures 14(12): 2123–2140, https://doi.org/10.1590/1679-78253616.

Bebiano, R., Camotim, D., & Gonçalves, R., (2018). GBTul 2.0 − A second-generation code for the GBT-based buckling and vibra tion analysis of thin-walled members. ThinWalled Structures 124:235–257, https://doi.org/10.1016/j.tws.2017.12.002.

Callesen, F. G., Blinkenberg-Thrane, M., Taylor, J. R., Kozine, I., (2021). Container ships: fire-related risks. Journal of Marine Eng ineering & Technology 20(4): 262-277, doi.org/10.1080/20464177.2019.1571672.

Cheung, Y. K., (1976). Finite strip method in structural analysis. vol. 3, no. 2. Adelaide: Pergamon Press.

EMSA Annual Overview of Marine Casualties and Incidents 2023. (2024). Available online: https://www.emsa.europa.eu/we-do/safety/accident-investigation/items.html?cid=141&id=5052.

Gao, D., Shi, G., Wang, D., (2012). Residual Ultimate Strength of Hull Structures with Crack and Corrosion Damage. Engineering Failure Analysis 25: 316–328, doi: 10.1016/j.engfailanal.2012.05.003.

Guedes Soares, C., Luís, R. M., Nikolov, P., Downes, J., Taczala, M., Modiga, M., Samuelides, M., (2008). Benchmark study on the use of simplified structural codes to predict the ultimate strength of a damaged ship hull. International Shipbuilding Progress 55(1-2): 87-107, doi: 10.3233/ISP-2008-0040.

Guo, Z., Chuang, M., Yi, L., (2023). Residual Strength Prediction and Structural Response of a Multi-Chamber Cabin to a Fire. Journal of Marine Engineering and Technology 22:294–303, doi:10.1080/20464177.2023.2233264.

IMO CASUALTY ANALYSIS PROCEDURE. (2004). Available online: https://wwwcdn.imo.org/localresources/en/OurWork/MSAS/Documents/CASUALTY%20ANALYSIS%20PROCEDURE.pdf

Krmek, I., Kos, S., & Brčić, D., (2022). Analytical research of the container ships cargo area fires in the period from 2010 to 2020 . NAŠE MORE: znanstveni časopis za more i pomorstvo 69(1), 62-69, doi:10.17818/NM/2022/1.8.

LAGRONE, S., (2021). Long Chain of Failures Left Sailors Unprepared to Fight USS Bonhomme Richard Fire, Investigation Finds. Available online: https://news.usni.org/2021/10/19/long-chain-of-failures-left-sailors-unprepared-to-fight-uss-bonhomme-richard-investigation-finds#jp-carousel-89259.

Larter, D., (2020).US Navy Orders General Dynamics Shipyard to Stop Work after Small Fire on the Warship Kearsarge Available online: https://www.defensenews.com/naval/2020/07/18/us-navy-orders-to-general-dynamics-nassco-to-stop-work-after-fire-on-uss-kearsarge/.

Lazzari, J. A. D., Batista, E. D. M., (2020). Distortional-Global Buckling Interaction Relevance in Cold-Formed Steel Lipped Chann el Columns. Latin American Journal of Solids and Structures 17(9), e332,doi:10.1590/1679-78256264.

Lazzari, J. A. de, Batista, E. de M., (2021). Finite strip method computer application for buckling analysis of thin-walled structur es with arbitrary cross-sections. REM - International Engineering Journal 74(3), 337–344. https://doi.org/10.1590/0370- 44672020740065

Leite, I. C. S., Silva, V. P., (2023). Effect of axial and rotational restraint on performance of composite beams with fire protection coating. Latin American Journal of Solids and Structures : 20(2), e481, doi:10.1590/1679-78257403

Lendon, B., (2024). Old aircraft carrier, once part of mighty Soviet fleet, burns in Chinese lagoon. Available online: https://edition.cnn.com/2024/08/19/china/old-soviet-aircraft-carrier-minsk-fire-china-intl-hnk-ml/index.html.

Li, C.F., Zhang, K., Wei, Z.Y., Guo, Z., Xu, W.J., (2021). Residual Strength of Hull Structures under Cabin Fire. Journal of Harbin Engineering University 42(05):610–617, doi:10.11990/jheu.201912040.

Lindemann, T., Kaeding, P. (2017). Application of the idealized structural unit method for ultimate strength analyses of stiffened plate structures. Ship technology research, 64(1), 15-29.

Liu, Y., Guo, Z., Jia, X., Li, C., Kang, J., (2022). Space Temperature Field and Structure Response of Multi-Chamber Cabin Subjected to Fire. Ocean Engineering 266:112904, doi: 10.1016/j.oceaneng.2022.112904.

Ma, Z., Pei, Z., Wu, W., (2022). Dynamic Ultimate Strength Analysis of Stiffened Plate Based on Idealized Structural Unit Method. Marine Structures 84: 103203, doi: 10.1016/j.marstruc.2022.103203.

Machado, L. R., Dutra, V. F. P., & Maghous, S. (2020). A limit analysis approach to the stability assessment of reinforced concrete panels in fire conditions. Latin American Journal of Solids and Structures 17(01), e247, doi:10.1590/1679-78255662.

Mei, J.X., Du Z.F., Zhu, H.T. Influencing Factors of Ultimate Strength of Stiffened Plate of Ship Structure. SHIP ENGINEERING 2021,43(09):37-42+64.DOI: 10.13788/j.cnki.cbgc.2021.09.08.

Moshtaghian A., Waldrop, T., (2020). 21 injured after an explosion and fire on a naval ship in San Diego. Available online: https://edition.cnn.com/2020/07/12/us/ship-explosion-san-diego-naval-base/index.html.

Paik, J.K., Ryu, M.G., He, K., Lee, D.H., Lee, S.Y., Park, D.K., Thomas, G., (2021). Full-Scale Fire Testing to Collapse of Steel Stiffened Plate Structures under Lateral Patch Loading (Part 1) – without Passive Fire Protection. Ships and Offshore Structures 16:227–242, doi:10.1080/17445302.2020.1764705.

Paik, J.K., Seo, J.K., Kim, D.M. (2006). Idealized Structural Unit Method and Its Application to Progressive Hull Girder Collapse Analysis of Ships. Ships and Offshore Structures 1: 235–247, doi:10.1533/saos.2006.0129.

R. Schardt, (1989) Verallgemeinerte Technische Biegetheorie (in German). Berlin, Heidelberg: Springer Berlin Heidelberg,

Ryu, M.G., He, K., Lee, D.H., Park, S.I., Thomas, G., Paik, J.K. (2021). Finite Element Modeling for the Progressive Collapse Analysis of Steel Stiffened-Plate Structures in Fires. Thin-Walled Structures 159:107262, doi: 10.1016/j.tws.2020.107262.

Sánchez Cruz, M. L., Carrillo, J., Almeida, S. F. M. D. (2016). Effect of thermal residual stresses on buckling and post-buckling properties of laminated composites perimetrally reinforced. Latin American Journal of Solids and Structures 13(3): 435-455, doi: 10.1590/1679-78251828.

Shi, G.J., Wang, D.Y., (2012). Ultimate strength model experiment regarding a container ship's hull structures. Ships and Offshore Structures 7(2), 165-184.

Smith, C.S., Davidson, P. C., Chapman, J. C., et al. (1975). Strength and stiffness of ship's plating under in-plane compression and tension. Journal of Ship Research 9(1):1-17.

Smith, S.C., (1977). Influence of Local Compressive Failure on Ultimate Longitudinal Strength of a Ship's, Hull. In Proceedings of the International Symposium on Practical Design in Shipbuilding (PRADS), Tokyo, Japan, 17–21 October: 73–79.

South African Maritime Safety Authority. (2024). Crew Rescued from OSV That Caught Fire Off South Africa. Available online: https://www.marinelink.com/news/crew-rescued-osv-caught-fire-off-south-517041.

Specification for Structural Steel Buildings: AISC 36005, (2005). American Institute of Steel Construction, Inc. Chicago, IL, USA.

Sri Lanka Ports Authority. (2024). Fire Breaks Out on Containership in Port of Colombo. Available online: https://www.marinelink.com/news/fire-breaks-containership-port-colombo-515924

Tan, K.H., Qian, Z.H., (2008). Experimental Behaviour of a Thermally Restrained Plate Girder Loaded in Shear at Elevated Temperature. Journal of Constructional Steel Research 64: 596–606, doi: 10.1016/j.jcsr.2007.12.008.

Ueda, Y., (2021). A Pioneer of Computational Welding Mechanics and Ultimate Strength Analysis (ISUM). Ships and Offshore Structures 16:11–30, doi:10.1080/17445302.2020.1855500.

Wang, L., Wang, J., Shi, M., Fu, S., Zhu, M. (2021). Critical risk factors in ship fire accidents. Maritime Policy & Management 48(6): 895-913, doi.org/10.1080/03088839.2020.1821110.

Wang, W., Lyu, X., Zhang, Y., Yu, Y., Zhang, T., (2020). Axial Compression Performance of Thin-Walled T-Shaped Concrete Filled Steel Tubular Columns under Constant High Temperature: Experimental and Numerical Study. Structures 27: 525–541, doi: 10.1016/j.istruc.2020.06.004.

Wu, J.X., Yan, M, Sun, X.W., (2024). Simplified Approach for Assessing the Explosive Residual Strength of Ship Hulls. Latin American Journal of Solids and Structures 21(10): e567, doi:10.1590/1679-78258339.

Wu, J.X., Du, Z.P., Yan, M., Sun, X.W., (2023). Assessment of Ship Hull Ultimate Strength under Fire Conditions: The Fire Smith Method Approach. Journal of Marine Science and Engineering 11: 2055, doi:10.3390/jmse11112055.